NANO LETTERS

Letter

pubs.acs.org/NanoLett

Bendable and Thin Sulfide Solid Electrolyte Film: A New Electrolyte Opportunity for Free-Standing and Stackable High-Energy All-Solid-State Lithium-Ion Batteries

Young Jin Nam,[†] Sung-Ju Cho,[†] Dae Yang Oh,[†] Jun-Muk Lim,[†] Sung Youb Kim,[‡] Jun Ho Song,[§] Young-Gi Lee,[∥] Sang-Young Lee,*[,†] and Yoon Seok Jung*[,†]

[†]School of Energy and Chemical Engineering, Department of Energy Engineering, and [‡]School of Mechanical and Advanced Materials Engineering, Ulsan National Institute of Science and Technology (UNIST), Ulsan 689-798, South Korea

[§]Advanced Batteries Research Center, Korea Electronics Technology Institute (KETI), 68 Yatap-dong, Bundang-gu, Seongnam-si, Gyeonggi-do 463-816, South Korea

[∥]Power Control Device Research Team, Electronics and Telecommunications Research Institute (ETRI), 218, Gajeongno, Yuseong-gu, Daejeon, 305-700, South Korea

S *Supporting Information*

ABSTRACT: Bulk-type all-solid-state lithium batteries (ASLBs) are considered a promising candidate to outperform the conventional lithium-ion batteries. Unfortunately, the current technology level of ASLBs is in a stage of infancy in terms of cell-based (not electrode-material-based) energy densities and scalable fabrication. Here, we report on the first ever bendable and thin sulfide solid electrolyte films reinforced with a mechanically compliant poly(paraphenylene terephthalamide) nonwoven (NW) scaffold, which enables the fabrication of free-standing and stackable ASLBs with high energy density and high rate capabilities. The ASLB, using a thin (~70 μm) NW-reinforced SE film, exhibits a 3-fold increase of the cell-energy-density compared to that of a conventional cell without the NW scaffold.

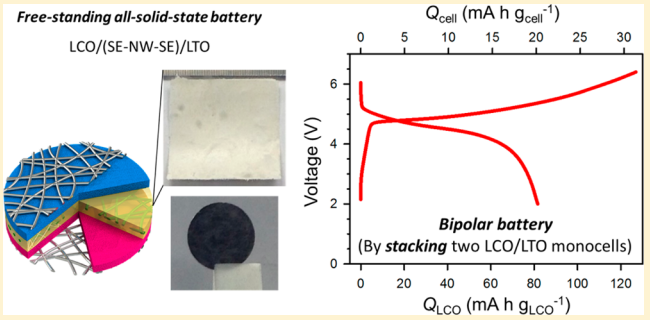

KEYWORDS: *All-solid-state lithium batteries, bendable sulfide solid electrolytes, composite materials, nonwovens, electrodes, nanostructures*

Commercialization of rechargeable lithium-ion batteries (LIBs) is attributed to the development of novel electrode materials ($LiCoO_2$/graphite), which enabled "rocking-chair" intercalation/deintercalation of lithium ions.[1,2] Optimization of the organic liquid electrolytes (LEs) that allow kinetically wide electrochemical windows and facile ion transport was also crucial to the success of LIBs.[1−3] Safety concerns arising from the organic LEs, including possible leakage and even fire/explosion have, however, seriously hindered the use of LIBs in large-scale energy storage applications such as electric vehicles and energy storage systems.[1−3]

Spurred by desperate demands for safe LIBs, all-solid-state lithium batteries (ASLBs) using noninflammable inorganic solid electrolytes (SEs) have attracted significant attention as ultimately safe energy storage device.[4,5] LiPON ($Li_{3.3}PO_{3.9}N_{0.17}$) is a well-known commercialized SE material and is used to fabricate thin-film-type ASLBs.[6] However, owing to its low room-temperature ionic conductivity in the range of ~10^{-6} S cm^{-1} and high preparation cost via vacuum deposition the application of thin-film-type ASLBs is limited to low energy devices such as smart cards and microelectronics.[6,7] In contrast, bulk-type ASLBs in which composite electrodes comprise a mixture of electrode materials, SE particles, and conductive carbon are considered to be fabricated by a scalable process and are especially promising for outperforming the conventional LIBs.[4,5,8−12] Oxide SE materials such as the perovskite $Li_{3x}La_{2/3-2x}\square_{1/3-2x}TiO_3$ ($0 < x < 0.16$) (LLTO)[13] and the garnet $Li_7La_3Zr_2O_{12}$ (LLZO)[14] exhibit high ionic conductivities of 10^{-4}−10^{-3} S cm^{-1} at room temperature and have been investigated for the fabrication of bulk-type ASLBs.[15−17] However, sintering at a high temperature of at least ~800 °C is necessary to form two-dimensional contacts between active materials and oxide SEs.[15−17] Unfortunately, high-temperature sintering deteriorates the interfaces between active materials and oxide SEs, leading to extremely poor electrochemical performances.[16] In sharp contrast, promising performances for bulk-type ASLBs have been reported using sulfide SE materials such as glass-ceramic Li_2S−P_2S_5 (e.g., $Li_7P_3S_{11}$ or $70Li_2S$-

Received: February 8, 2015
Revised: April 13, 2015
Published: April 28, 2015

DOI: 10.1021/acs.nanolett.5b00538
Nano Lett. 2015, 15, 3317−3323

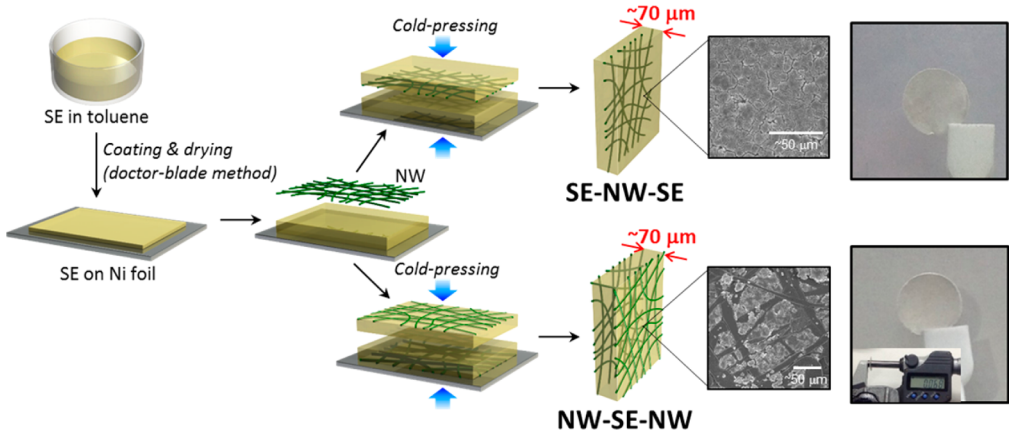

Figure 1. Schematic diagram showing the fabrication of bendable sulfide NW-SE films with two different structures (SE-NW-SE and NW-SE-NW). FESEM and photo images are also provided.

$30P_2S_5$: 1.7×10^{-2} S cm^{-1} at maximum),[18,19] thio-LISICON ($Li_{3.25}Ge_{0.25}P_{0.75}S_4$),[20] and $Li_{10}GeP_2S_{12}$ (LGPS, 1.2×10^{-2} S cm^{-1}).[4] Even though sulfide SE materials suffer from instability in air (due to generation of toxic H_2S gas when reacting with moisture in air),[21] the investigation of ASLBs using sulfide SEs has been accelerated because sulfide SEs are far superior to their oxide counterparts in terms of the following properties: First, sulfide SEs exhibit higher ionic conductivities than oxide SEs.[4,18−20] Especially, realization of extremely high conductivities for LGPS (1.2×10^{-2} S cm^{-1})[4] and its family of materials, such as $Li_{10}SnP_2S_{12}$ (4×10^{-2} S cm^{-1}),[22] even comparable to that of organic LEs (~10^{-2} S cm^{-1}), has been considered a breakthrough.[18−20] Second, the sulfide SE is ductile, exhibiting Young's moduli in between those of organic polymers and oxide ceramics, which enables intimate contacts with active materials by means of a simple cold pressing procedure.[8,23]

To date, many studies of ASLBs have focused on investigating the electrode chemistries.[4,8,9,24−31] Conventional electrode materials used for LIBs, such as Li_xMO_2 (M = Co, Ni, Mn),[4,8,9,24,25] graphite,[8,26] and $Li_4Ti_5O_{12}$,[27] have been investigated for application in ASLBs. High-capacity sulfur-[28,29] or Li_2S-based[30,31] composite electrodes have also been developed for application to ASLBs. However, their highly insulating characteristics and large changes in dimension upon insertion/extraction of lithium ions pose critical challenges to realizing ASLBs with reliable and sustainable electrochemical properties.[28,30,32] In contrast, the high operating voltage (~4 V vs Li/Li$^+$), low volume change during charge−discharge (e.g., 1.9% for $LiCoO_2$),[33] and moderate electrical conductivity of the conventional Li_xMO_2 (e.g., ~10^{-3} S cm^{-1} for $LiCoO_2$ and ~20 S cm^{-1} for $Li_{0.5}CoO_2$)[34] make Li_xMO_2 well-suited for application in ASLBs. Li_xMO_2 has poor compatibility with sulfide SE, however, and a variety of surface modification treatments (in particular, metal oxide coatings) have been performed on Li_xMO_2 in order to overcome this drawback.[4,8,9,24,25,35] Other than protective coatings, while the surface chemistry of bare Li_xMO_2 is also known to be important for the performance of conventional liquid electrolyte cells,[36−38] investigations on the performance of bare Li_xMO_2 by varying the surface chemistry are rare for ASLBs.

Unfortunately, most of the previous studies of ASLBs have not paid much attention to cell-based (not electrode-material-based) energy densities, which are far too low to compete with those of conventional LIBs. ASLBs contain excessively large amounts of SE which nullify the advantages of using high-energy electrode materials. Approximately 30−70 wt % of SEs are used in the composite electrodes,[4,5,8,9,12,23,27,30,39] which, conversely, results in a 30−70% decrease in the corresponding energy density based on composite electrodes. In order to minimize the amount of SE in the composite electrodes, laser vapor deposition was used to directly coat the active materials ($LiCoO_2$ (LCO)) with SE thereby forming intimate contacts between the two.[8,35] Recently, wet chemical methods have also been investigated for depositing SE layers on active materials.[40] More importantly, it should be noted that the typical lab-made pellet-type ASLBs consist of a very thick (~0.5−1.0 mm) SE layer with a mass loading in the range of ~90−150 mg cm^{-2};[5,8,9,11,12,25,27,29,30,41] this very thick SE layer results, undoubtedly, in a significant decrease in the energy density of the cell.

From the viewpoint of cell energy density and scalable fabrication, the technology level of ASLBs is also in a stage of infancy. For example, the literature consists of only a few reports to date on sheet-type ASLBs such as the Mo_6S_8/Li−Al battery with thio-LISICON ($Li_{3.25}Ge_{0.25}P_{0.75}S_4$)[42] and the $LiNi_{0.80}Co_{0.15}Al_{0.05}O_2$/graphite battery with $80Li_2S$-$20P_2S_5$.[43]

Here, we report on the first ever bendable and thin sulfide SE films reinforced with a mechanically compliant poly(paraphenylene terephthalamide) (PPTA) nonwoven (NW) scaffold, which enables the fabrication of free-standing and stackable ASLBs with high energy and high rate capabilities. The free-standing and stackable ASLB consists of a $LiCoO_2$ cathode, a $Li_4Ti_5O_{12}$ anode, and a thin (~70 μm) NW-reinforced SE (referred as "NW-SE" hereafter) film; the $LiCoO_2$ has a clean surface that was prepared by heat-treating in air. Furthermore, by incorporating the bendable NW-SE film, the cell energy density of the ASLB is increased by a factor of 3 compared to that of the conventional cell that does not contain NW.

The fabrication process of the NW-SE films is illustrated in Figure 1. The sulfide SE used was either glass-ceramic Li_3PS_4 (LPS, pristine, 1.0×10^{-3} S cm^{-1} at 30 °C, after exposure to anhydrous toluene, 7.3×10^{-4} S cm^{-1}) or tetragonal $Li_{10}GeP_2S_{12}$ (LGPS, pristine, 6.0×10^{-3} S cm^{-1} at 30 °C, after exposure to anhydrous toluene, 4.0×10^{-3} S cm^{-1}).[39] Fabrication of the films begins with using the doctor-blade method to coat the sulfide SE slurry (using anhydrous toluene as a solvent) on a Ni foil and involves subsequent drying. The as-prepared SE-coated Ni foil is then cold-pressed onto the NW substrate. This pressing results in the transfer of the SE layer

DOI: 10.1021/acs.nanolett.5b00538
Nano Lett. 2015, 15, 3317−3323

Table 1. Major Characteristics of the NW-SE Films

name of SE films	conductivity (mS cm^{-1})	E_a (kJ mol^{-1})	thickness (μm)	mass loading (mg cm^{-2})	conductance (mS)
LPS[a]	0.73	26.0	700	110	14
LPS-NW-LPS	0.20	31.0	70	5.7	37
NW-LPS-NW	0.16	49.2	70	5.7	29
LGPS-NW-LPS	0.34	24.8	90	11[b]	50
NW-LGPS-LPS-NW	0.20	44.0	90	11[b]	20

[a]For fair comparison with the NW-SE films, the LPS SE powders were exposed to anhydrous toluene. [b]Weight ratio of LGPS/LPS is 1.4.

from the Ni foil to the NW substrate owing to the better adhesion of the SE layer toward the NW substrate than the Ni foil. Two different configurations ("SE-NW-SE" and "NW-SE-NW") of the NW-SE films were prepared via this "transfer" method. Even though a "SE-NW" film can also be fabricated, in this work, only films with a symmetric configuration were used for reasonable evaluation in further electrochemical tests. The as-prepared SE-NW-SE and NW-SE-NW films are both free-standing, have a mass loading of ~5.7 mg cm^{-2} and are ~70 μm thick. In addition, the PPTA NW is very light (0.8 mg cm^{-2}) and constitutes only 14% of the mass of the NW-SE film (SE-NW-SE). This PPTA NW, which is known as a high-performance polymer with good thermal, chemical, and electrochemical stability,[44,45] serves as a mechanically compliant scaffold that provides flexibility and toughness to the NW-SE film. Especially, the PPTA NW is stable up to ~400 °C (Supporting Information Figure S1), which demonstrates that the inclusion of organic component, PPTA NW, does not significantly degrade the intrinsic advantage of excellent thermal stability of sulfide SEs. With a thickness of only 16 μm, the PPTA NW is also thin and has a high porosity (70%) as well as large opening sizes (~40 μm) (Supporting Information Figure S2). These features allow easy penetration of the sulfide SE particles into the pores of the PPTA NW, as evidenced by the merged SE materials observed at the openings of the NW of the NW-SE-NW film in Figure 1. Moreover, the marginal decrease in conductivity values (Table 1) of the NW-SE films (0.20 mS cm^{-1} for LPS-NW-LPS and 0.16 mS cm^{-1} for NW-LPS-NW) compared to those of conventional SE films (0.73 mS cm^{-1}) confirms that good ionic conduction pathways formed in the SE materials that were impregnated inside the NW scaffold. Note, however, that the conductance values of the NW-SE films (37 mS for LPS-NW-LPS and 29 mS for NW-LPS-NW) are higher than that of the conventional SE film (14 mS). The comparison of the conductivity and conductance values shown in Table 1 will be further discussed in a later section. In a previous report,[39] our group demonstrated that by using a LGPS-LPS SE bilayer in which LPS faces the Li–In anode (operating voltage, ~0.62 V vs Li/Li$^+$ for In + Li$^+$ + e$^-$ ↔ LiIn), it is possible to overcome the poor stability problem of $Li_{10}GeP_2S_{12}$ (LGPS) in contact with Li–In with exploiting the high conductivity of $Li_{10}GeP_2S_{12}$ (LGPS) in the TiS_2/Li–In all-solid-state cell. A thin and free-standing bilayer NW-SE film, which consists two different SE layers and NW, and thereby allows wide electrochemical window with retaining high ionic conductivity, can also be fabricated by using the "transfer" method. For example, a free-standing LGPS-LPS bilayer SE film can be fabricated as combinations of LPS-NW-LGPS or NW-LGPS-LPS-NW (Table 1).

Figure 2a compares photo images of the SE films, with and without the NW scaffold, immediately after cold-pressing. As evidenced by the cracks (indicated by the arrow) formed, cold-pressing resulted in severe mechanical failure of the 470 μm

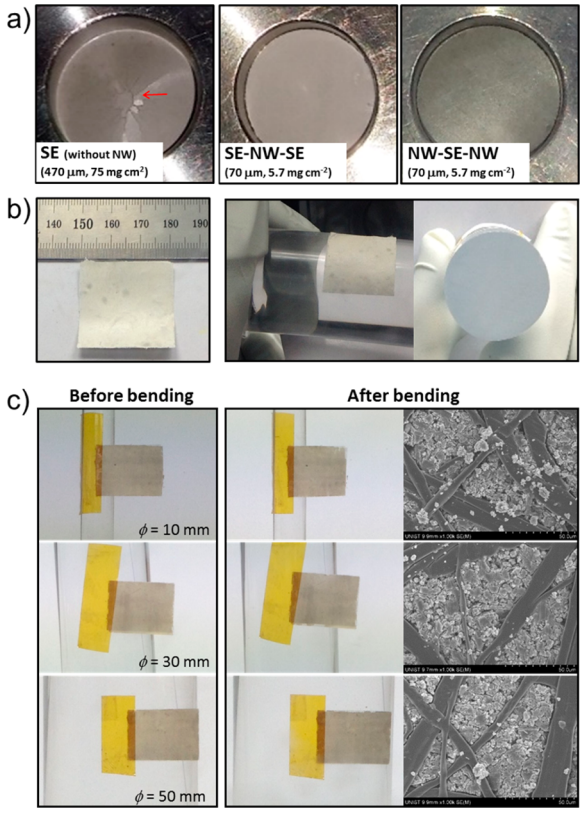

Figure 2. (a) Photo images of the conventional SE pellet and bendable NW-SE films. The pellets have a diameter of 1.3 cm. Note the cracks in the conventional SE pellet, as indicated by the arrow. (b) Photo images of 3 × 3 cm^2 bendable NW-SE films (NW-SE-NW). (c) Photo and FESEM images of 1.5 × 2.0 cm^2 bendable NW-SE films (NW-SE-NW) before and after bending tests. The diameter of rods is provided. Li_3PS_4 (LPS) was used as the SE.

thick conventional Li_3PS_4 SE film. Considering that the diameter of pellet is only 1.3 cm, it should be emphasized that this mechanical failure must be critically severer when the SE films with larger dimension are fabricated for scalable production. In sharp contrast, the SE-NW-SE and NW-SE-NW SE films remained intact during cold-pressing. Although sulfide materials are ductile, cold-pressing is insufficient for the formation of pore-free SE monoliths. In fact, field emission scanning electron microscopy (FESEM) images (Supporting Information Figure S3) revealed the presence of voids between the merged particles of the cold-pressed LPS SE pellets. The pellets were found to have a porosity of 14–17% as determined by calculations based on the comparison of the apparent, that is, from the crystallographic data,[46,47] and the measured densities (Supporting Information). The mechanical failure of conventional SE films without the NW scaffold in Figure 2a originates from the aforementioned mechanical imperfection. It

DOI: 10.1021/acs.nanolett.5b00538
Nano Lett. 2015, 15, 3317–3323

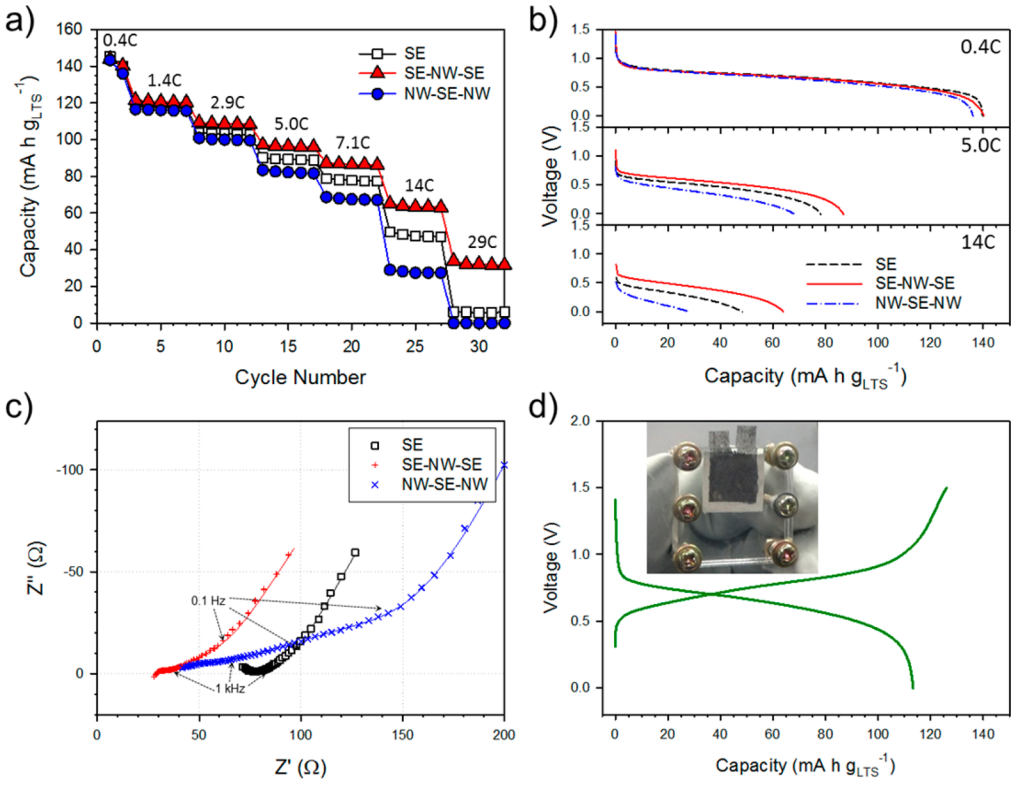

Figure 3. (a) Variations in discharge capacities versus cycle number, (b) discharge voltage profiles at different C-rates, and (c) Nyquist plots of $LiTiS_2/Li_4Ti_5O_{12}$ (LTS/LTO) all-solid-state cells using the conventional SE pellet and bendable NW-SE films as the SE layer at 30 °C. The solid lines indicate the fitting results using Voigt-type equivalent circuit model (Supporting Information Figure S5). 1C-rate is 140 mA g_{LTS}^{-1} (= 0.16 mA cm^{-2}). (d) First charge−discharge voltage profiles of the prototype free-standing LTS/LTO sheet battery at 89 μA cm^{-2} at 30 °C. A photo image of the LTS/LTO sheet battery is shown in the inset.

is thought that breakage of the pellet, which is initiated at the microstructural defects or voids by the strain caused by cold-pressing, is accelerated in insufficiently thick SE films. In contrast, owing to the highly flexible NW scaffold, the as-prepared NW-SE-NW film is both free-standing and bendable and, as such, can be easily wound around a 3 cm diameter rod (Figure 2b). The mechanical integrity of the NW-SE-NW films upon repeated bending was assessed by bending the 1.5 × 2.0 cm^2 films ten times around rods with diameters of 1, 3, and 5 cm; the results are shown in Figure 2c. It was observed that while the contacts among SE particles and between SE particles and NW frameworks were slightly loosened and some SE particles were detached on bending around the 1 cm rod, the structural integrity was retained on bending around the 3 and 5 cm rods, demonstrating the excellent mechanical flexibility of the composite film. The excellent bendability is also demonstrated in a movie clip (Supporting Information Movies S1). To our best knowledge, this work is the first report on flexible inorganic SE films with significant bendability. It should be emphasized that the free-standing feature or bendability of the NW-SE films could provide a viable option to allow roll-to-roll processes. In addition, the technology used to fabricate the NW-SE films has the potential to ultimately realize bendable bulk-type all-solid-state batteries based on inorganic SEs,[48,49] which will be our next mission.

As Table 1 shows, the bendable NW-SE films have lower conductivity values than those of their conventional SE counterparts, which is not surprising because the NW scaffold is not Li^+-ion conductive. As demonstrated, however, the use of NW allows the fabrication of very thin (~70 μm) bendable composite films (Figures 1 and 2), which appear to have higher conductance values than those of the conventional thick SE film (Table 1 and Supporting Information Table S1). All-solid-state cells incorporating $LiTiS_2$ (LTS) and $Li_4Ti_5O_{12}$ (LTO) as the cathode and anode, respectively were fabricated in order to make a fair assessment of the benefit of the high conductance of the bendable NW-SE films. LTS and LTO operate at mild voltages (~2.1 V vs Li/Li^+ for LTS and ~1.6 V vs Li/Li^+ for LTO) (Supporting Information Figure S4) and thus their use of nanosized particles is not problematic. As such, the charge transfer resistance at the electrode−electrolyte interfaces and Li^+-ion diffusion in the bulk are expected to have inappreciable effect on the overall rate performance.[50]

Figure 3 compares the electrochemical performance of the LTS/LTO all-solid-state cells containing the conventional SE film ("SE") to that of the bendable NW-SE films (SE-NW-SE and NW-SE-NW). In contrast to the cell with conventional SE film that has negligible capacity at high C-rates, that is, ~32 mA h g_{LTS}^{-1} at 29C (4.4 mA cm^{-2}), the cell with SE-NW-SE film exhibits lower polarization and thus higher capacities. This enhanced rate performance is attributed to the higher ionic conductance of the latter (37 mS) compared to that of the former (14 mS) (Table 1). Electrochemical impedance spectroscopy (EIS) results of the LTS/LTO cell also show that the intercept values at the Z' axis in the Nyquist plots (Figure 3c), which are interpreted as resistance of the SE layers,[11,23,39] of the SE-NW-SE and NW-SE-NW cells are lower than that of the cell with the conventional SE. However, the rate capability of the cell with the NW-SE-NW film is slightly inferior to that of the conventional cell. The Nyquist plots in

DOI: 10.1021/acs.nanolett.5b00538
Nano Lett. 2015, 15, 3317−3323

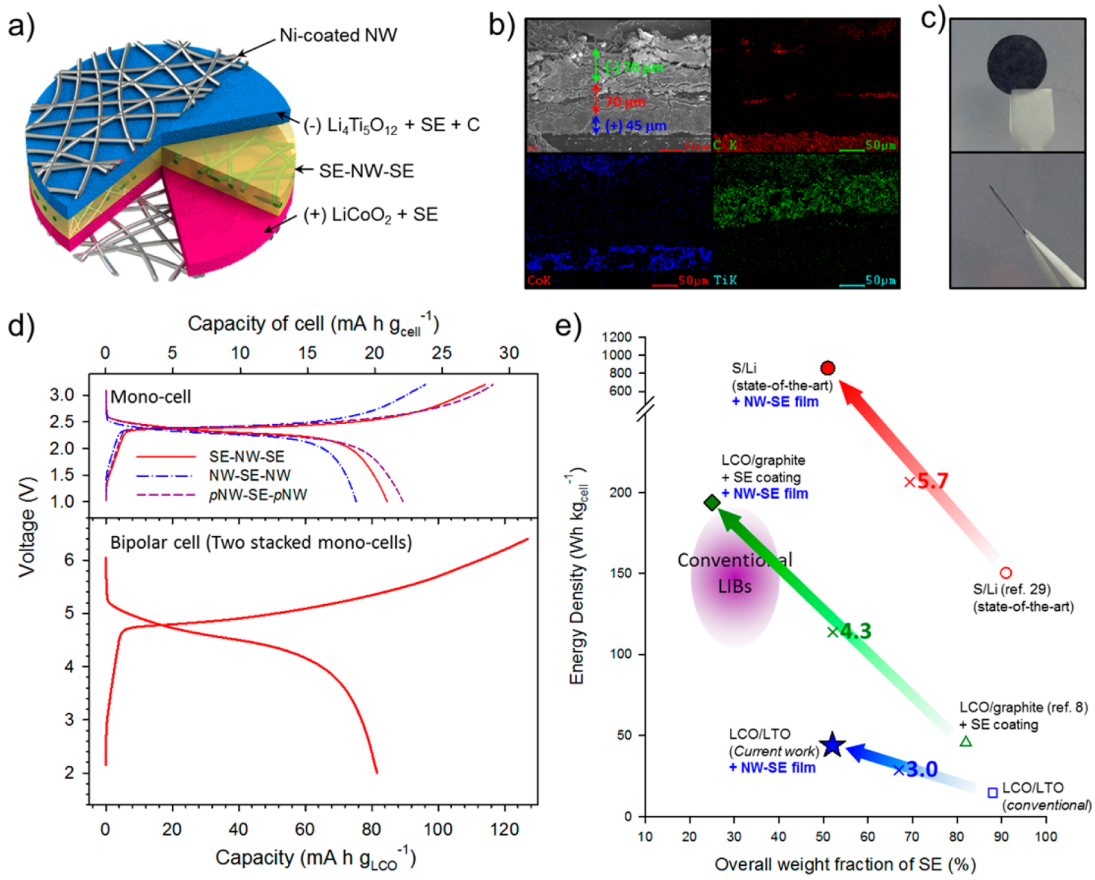

Figure 4. (a) Schematic diagram, (b) cross-sectional FESEM image and EDS elemental maps, and (c) photo images of the free-standing $LiCoO_2$/(SE-NW-SE)/$Li_4Ti_5O_{12}$ (LCO/(SE-NW-SE)/LTO) all-solid-state cell. (d) First charge−discharge voltage profiles of the free-standing LCO/LTO all-solid-state monocells with different-structured SE films (SE-NW-SE, NW-SE-NW, pNW-SE-pNW) and the free-standing bipolar cell constructed by stacking two free-standing monocells (LCO/(SE-NW-SE)/LTO) at 14 mA g_{LCO}^{-1} (= 0.11 mA cm^{-2}) at 30 °C. (e) Comparison of the energy densities of the all-solid-state battery as a function of the overall weight fraction of SEs varied by electrode chemistry, the presence of SE coating, and the bendable NW-SE film.

Figure 3c show that the data in midfrequency ranges for the cell containing NW-SE-NW exhibit more depressed shape than others (SE and SE-NW-SE). This indicates that the cell containing NW-SE-NW has a higher charge transfer resistance compared to that of the other two cells. Fitting of the EIS data using a Voigt-type equivalent circuit model[51] (Supporting Information Figure S5) results in overall charge transfer resistances of 5.4 Ω, 7.2 Ω, and 143 Ω for the SE, SE-NW-SE, and NW-SE-NW cells, respectively. The suppressed charge transfer kinetics may have resulted from blocking of the ionic conduction between the active materials and the SE by the nonconductive NW scaffold at the composite electrode−SE interface, which explains the inferior rate capability of the NW-SE-NW cell compared to the conventional SE cell (Figure 3a,b), despite the higher conductance of NW-SE-NW (29 mS) compared to SE (14 mS) (Table 1). Future work will include development of a Li-ion conducting NW scaffold in order to further enhance the rate performance of NW-SE-containing cells. A prototype 1.5 × 1.5 cm^2 free-standing LTS/(SE-NW-SE)/LTO sheet battery was fabricated and its reversible electrochemical behavior is also demonstrated in Figure 3d.

In addition, LCO and LTO were selected as cathode and anode, respectively, in order to examine the performance of high-energy all-solid-state cells which incorporate the bendable SE films. High mass-loading of LCO (LCO/LGPS = 70:30 wt %) was performed in order to maximize the cell energy density. The pristine LCO in LCO/Li−In cell exhibits a first discharge capacity of only 8 mA h g_{LCO}^{-1} at 0.1C (14 mA g_{LCO}^{-1} = 0.11 mA cm^{-2}) (Supporting Information Figure S6a). Surprisingly, the use of heat-treated (at 800 °C in air) LCO significantly improves the electrochemical performance, resulting in a first discharge capacity of 121 mA h g_{LCO}^{-1} (Supporting Information Figure S6a). In previous literature related to LE-based LIBs, it was argued that improvements of performance in LCO by metal-oxides coatings is due to elimination of impurities such as LiOH and Li_2CO_3 during the heat-treatment used for the wet-coating procedures rather than the protective role of metal-oxide coatings.[36−38] In ASLBs, the surface impurities may block the transport of Li ions between the SE and the LCO particles with whom they contact. This blocking results in a huge impedance and thus negligible capacity, which is verified by the significantly higher amount of Li_2CO_3 in the pristine LCO (4400 ppm) than in the heat-treated LCO (1000 ppm). Even if the electrochemical performance of LCO depending on the surface chemistry is important, it is beyond the scope of current work.

By combination of the heat-treated LCO with the SE-NW-SE (or NW-SE-NW) film and Ni-coated NW (acting as a flexible current collectors), a free-standing LCO/LTO all-solid-state cell was fabricated. The cell structure is depicted in Figure 4a. Figure 4b and Supporting Information Figure S7 show that the cell has an overall thickness ∼185 μm and the photo images in

DOI: 10.1021/acs.nanolett.5b00538
Nano Lett. 2015, 15, 3317−3323

Figure 4c demonstrate the corresponding free-standing characteristics. Figure 4d represents the voltage profiles of the free-standing LCO/LTO all-solid-state cells. The corresponding cycle performances are also shown in Supporting Information Figure S8. The composite cathode (15 mg cm^{-2}) and anode (24 mg cm^{-2}) include 70.0 wt % of LCO and 49.8 wt % of LTO, respectively. The SE-NW-SE and NW-SE-NW cells had respective first discharge capacities of 85 and 75 mA h g_{LCO}^{-1}. The lower capacity of the latter, compared to the former, is considered to arise from poor ionic contacts at the LCO cathode/(NW-SE-NW) interface. In order to improve the capacity, a polymer electrolyte consisting of LiTFSI (lithium bis(trifluoromethanesulfonyl)imide) with PEO (poly(ethylene oxide)) was coated on the NW scaffold, yielding a PEO/LiTFSI-coated NW scaffold denoted as "pNW". The presence of a coating layer was confirmed not only by the elemental maps of the as-prepared pNW obtained by FESEM analysis (Supporting Information Figure S9a) but also by the HRTEM results of the cross-sectioned pNW obtained using focused ion beam (FIB) etching (Supporting Information Figure S9b). Especially, the HRTEM results in Supporting Information Figure S9b show that the coating layer is uniform and has an estimated thickness of 20−40 nm. As seen in Figure 4d, the first discharge capacity of the LCO/LTO cell incorporating the pNW, pNW-SE-pNW, is significantly higher (89 mA h g_{LCO}^{-1} vs 75 mA h g_{LCO}^{-1}) than that of the NW-SE-NW. The respective first discharge capacities of the SE-NW-SE and pNW-SE-pNW LCO/LTO cells, 85 and 89 mA h g_{LCO}^{-1}, translate to energy density values of 42 and 44 Wh kg_{cell}^{-1}. Figure 4e shows the cell energy density of all-solid-state cells as a function of the overall weight fraction of SE. The energy density obtained in this work (44 Wh kg_{cell}^{-1}) is still much lower than that (100−200 Wh kg_{cell}^{-1}) of commercialized LIBs[52] and also some conventional ASLB adopting high-capacity electrode materials such as sulfur (e.g., ∼150 Wh kg_{cell}^{-1} assuming that Li metal can be used.). It should be noted, however, that by applying the bendable and thin NW-SE film, the energy density of the LCO/LTO ASLB was almost three times higher than that of the conventional ASLB (15 Wh kg_{cell}^{-1}) that does not contain NW. If novel electrode chemistry such as sulfur[20] and/or an SE-coated electrode materials[8,35] is combined with the NW-SE film, further improvement in the energy density is highly expected. For example, consider the case of an NW-SE film sandwiched between LCO and graphite composite electrodes in which the electrode powders are coated by 10 wt % of SE via a pulsed laser deposition method.[8] The overall weight fraction of SE would be reduced to as low as ∼25 wt % and the cell energy density would be increased to ∼190 Wh kg_{cell}^{-1}, that is, 4.3 times that of the original NW-SE film. This value (∼190 Wh kg_{cell}^{-1}) is comparable to the values for conventional LIBs that use LEs.[51] In addition, an energy density of over 860 Wh kg_{cell}^{-1} is expected if an ASLB were to be composed of the state-of-the-art sulfur cathode[29] and a Li anode that contains the NW-SE film. This value (860 Wh kg_{cell}^{-1}) would represent a 5.7-fold increase compared to that of the non-NW-containing cell and far exceeds that of the conventional LIBs.

The free-standing feature of the (NW-SE)-incorporated ASLB also facilitates stacking of monocells. Voltages can be easily doubled or tripled via simple stacking of precharged $Li_{1-x}CoO_2/Li_{4+x}Ti_5O_{12}$ monocells (Supporting Information Movie S2). In addition, capacities of the free-standing bipolar cell constructed by stacking two free-standing monocells (LCO/(SE-NW-SE)/LTO) are comparable to those of the monocell, as demonstrated in the first charge−discharge voltage profiles (Figure 4c). In contrast, for the conventional LIBs using LEs achieving targeted high voltages of battery packs (e.g., tens of V) is possible only through serial connections of each fully packaged monocell. Considering weight of cell-packaging, the overall cell energy density increases with increasing number of monocells stacked in the ASLBs.

In conclusion, we have demonstrated the facile and scalable fabrication of bendable and thin (∼70 μm) sulfide SE films reinforced with a mechanically compliant NW-scaffold and their application for free-standing and stackable ASLBs. By incorporating the pNW-SE film, the cell energy density of the LCO/LTO all-solid-state cell increased by approximately a factor of 3 (to 44 Wh kg_{cell}^{-1}), compared to that of the conventional all-solid-state cell without the NW scaffold. Improved rate capabilities were also achieved for the LTS/LTO all-solid-state cells that contain the NW-SE films. We believe that the NW-SE films proposed herein hold significant promise as a compelling building unit and their combination with the elaborately designed cell architecture provides a new route for the development of high-performance ASLBs.

■ ASSOCIATED CONTENT

Supporting Information

Experimental methods and supplementary results. The Supporting Information is available free of charge on the ACS Publications website at DOI: 10.1021/acs.nanolett.5b00538.

■ AUTHOR INFORMATION

Corresponding Authors

*E-mail: syleek@unist.ac.kr.
*E-mail: ysjung@unist.ac.kr.

Author Contributions

The manuscript was written through contributions of all authors. All authors have given approval to the final version of the manuscript.

Y.J.N. and S.-J.C. contributed equally.

Notes

The authors declare no competing financial interest.

■ ACKNOWLEDGMENTS

This work was supported by the Energy Efficiency & Resources Program of the Korea Institute of Energy Technology Evaluation and Planning (KETEP) grant funded by the Korea government Ministry of Trade, Industry & Energy (No. 20112010100150) and by Basic Science Research Program through the National Research Foundation of Korea (NRF) funded by the Ministry of Education (No. NRF-2014R1A1A2058760).

■ ABBREVIATIONS

ASLB, all-solid-state lithium battery; LIB, lithium-ion battery; SE, solid-electrolyte; PPTA, poly(paraphenylene terephthalamide); LCO, $LiCoO_2$; LTO, $Li_4Ti_5O_{12}$; NW, nonwoven; LPS, Li_3PS_4; LGPS, $Li_{10}GeP_2S_{12}$; PEO, poly(ethylene oxide); LiTFSI, lithium bis(trifluoromethanesulfonyl)imide; HRTEM, high-resolution transmission electron microscopy; FIB, focused ion beam

DOI: 10.1021/acs.nanolett.5b00538
Nano Lett. 2015, 15, 3317−3323

REFERENCES

(1) Goodenough, J. B.; Kim, Y. *Chem. Mater.* **2010**, *22*, 587−603.
(2) Tarascon, J.-M.; Armand, M. *Nature* **2001**, *414*, 359−367.
(3) Xu, K. *Chem. Rev.* **2004**, *104*, 4303−4417.
(4) Kamaya, N.; Homma, K.; Yamakawa, Y.; Hirayama, M.; Kanno, R.; Yonemura, M.; Kamiyama, T.; Kato, Y.; Hama, S.; Kawamoto, K.; Mitsui, A. *Nat. Mater.* **2011**, *10*, 682−686.
(5) Jung, Y. S.; Oh, D. Y.; Nam, Y. J.; Park, K. H. *Israel J. Chem.* **2015**, DOI: 10.1002/ijch.201400112.
(6) Wang, B.; Bates, J. B.; Hart, F. X.; Sales, B. C.; Zuhr, R. A.; Robertson, J. D. *J. Electrochem. Soc.* **1996**, *143*, 3203−3213.
(7) Patil, A.; Patil, V.; Shin, D. W.; Choi, J.-W.; Paik, D.-S.; Yoon, S.-J. *Mater. Res. Bull.* **2008**, *43*, 1913−1942.
(8) Sakuda, A.; Hayashi, A.; Tatsumisago, M. *Sci. Rep.* **2013**, *3*, 2261.
(9) Ohta, N.; Takada, K.; Zhang, L.; Ma, R.; Osada, M.; Sasaki, T. *Adv. Mater.* **2006**, *18*, 2226−2229.
(10) Lin, Z.; Liu, Z.; Fu, W.; Dudney, N. J.; Liang, C. *Angew. Chem., Int. Ed.* **2013**, *52*, 7460−7463.
(11) Shin, B. R.; Nam, Y. J.; Kim, J. W.; Lee, Y.-G.; Jung, Y. S. *Sci. Rep.* **2014**, *4*, 5572.
(12) Yersak, T. A.; Macpherson, H. A.; Kim, S. C.; Le, V.-D.; Kang, C. S.; Son, S.-B.; Kim, Y.-H.; Trevey, J. E.; Oh, K. H.; Stoldt, C.; Lee, S.-H. *Adv. Energy Mater.* **2013**, *3*, 120−127.
(13) Stramare, S.; Thangadurai, V.; Weppner, W. *Chem. Mater.* **2003**, *15*, 3974−3990.
(14) Murugan, R.; Thangadurai, V.; Weppner, W. *Angew. Chem., Int. Ed.* **2007**, *46*, 7778−7781.
(15) Kotobuki, M.; Munakata, H.; Kanamura, K.; Sato, Y.; Yoshida, T. *J. Electrochem. Soc.* **2010**, *157*, A1076−A1079.
(16) Kim, K. H.; Iriyama, Y.; Yamamoto, K.; Kumazaki, S.; Asaka, T.; Tanabe, K.; Fisher, C. A. J.; Hirayama, T.; Murugan, R.; Ogumi, Z. *J. Power Sources* **2011**, *196*, 764−767.
(17) Ohta, S.; Seki, J.; Yagi, Y.; Kihira, Y.; Tani, T.; Asoka, T. *J. Power Sources* **2014**, *265*, 40−44.
(18) Mizuno, F.; Hayashi, A.; Tadanaga, K.; Tatsumisago, M. *Adv. Mater.* **2005**, *17*, 918−921.
(19) Seino, Y.; Ota, T.; Takada, K.; Hayashi, A.; Tatsumisago, M. *Energy Environ. Sci.* **2014**, *7*, 627−631.
(20) Kanno, R.; Murayama, M. *J. Electrochem. Soc.* **2001**, *148*, A742−A746.
(21) Muramatsu, H.; Hayashi, A.; Ohtomo, T.; Hama, S.; Tatsumisago, M. *Solid State Ionics* **2011**, *182*, 116−119.
(22) Bron, P.; Johansson, S.; Zick, K.; auf der Guenne, J. S.; Dehnen, S.; Roling, B. *J. Am. Chem. Soc.* **2013**, *135*, 15694−15697.
(23) Shin, B. R.; Jung, Y. S. *J. Electrochem. Soc.* **2014**, *161*, A154−A159.
(24) Woo, J. H.; Trevey, J. E.; Cavanagh, A. S.; Choi, Y. S.; Kim, S. C.; George, S. M.; Oh, K. H.; Lee, S.-H. *J. Electrochem. Soc.* **2012**, *159*, A1120−A1124.
(25) Sakuda, A.; Hayashi, A.; Tatsumisago, M. *Chem. Mater.* **2010**, *22*, 949−956.
(26) Takada, K.; Inaba, T.; Kajiyama, A.; Sasaki, H.; Kondo, S.; Watanabe, M.; Murayama, M.; Kanno, R. *Solid State Ionics* **2003**, *158*, 269−274.
(27) Kitaura, H.; Hayashi, A.; Tadanaga, K.; Tatsumisago, M. *J. Electrochem. Soc.* **2009**, *156*, A114−A119.
(28) Nagao, M.; Hayashi, A.; Tatsumisago, M. *Energy Technol.* **2013**, *1*, 186−192.
(29) Nagata, H.; Chikusa, Y. *J. Power Sources* **2014**, *264*, 206−210.
(30) Nagao, M.; Hayashi, A.; Tatsumisago, M. *J. Mater. Chem.* **2012**, *22*, 10015−10020.
(31) Lin, Z.; Liu, Z.; Dudney, N. J.; Liang, C. *ACS Nano* **2013**, *7*, 2829−2833.
(32) Ji, X. L.; Lee, K. T.; Nazar, L. F. *Nat. Mater.* **2009**, *8*, 500−506.
(33) Koyama, Y.; Chin, T. E.; Rhyner, U.; Holman, R. K.; Hall, S. R.; Chiang, Y. M. *Adv. Funct. Mater.* **2006**, *16*, 492−498.
(34) Sauvage, F.; Tarascon, J.-M.; Baudrin, E. *J. Phys. Chem. C* **2007**, *111*, 9624−9630.
(35) Sakuda, A.; Hayashi, A.; Ohtomo, T.; Hama, S.; Tatsumisago, M. *Electrochem. Solid-State Lett.* **2010**, *13*, A73−A75.
(36) Chen, Z.; Dahn, J. R. *Electrochem. Solid-State Lett.* **2003**, *6*, A221−A224.
(37) Chen, Z.; Dahn, J. R. *Electrochem. Solid-State Lett.* **2004**, *7*, A11−A14.
(38) Liu, H. S.; Zhang, Z. R.; Gong, Z. L.; Yang, Y. *Electrochem. Solid-State Lett.* **2004**, *7*, A190−A193.
(39) Shin, B. R.; Nam, Y. J.; Oh, D. Y.; Kim, D. H.; Kim, J. W.; Jung, Y. S. *Electrochim. Acta* **2014**, *146*, 395−402.
(40) Teragawa, S.; Aso, K.; Tadanaga, K.; Hayashi, A.; Tatsumisago, M. *J. Power Sources* **2014**, *248*, 939−942.
(41) Yersak, T. A.; Trevey, J. E.; Lee, S. H. *J. Power Sources* **2011**, *196*, 9830−9834.
(42) Inada, T.; Kobayashi, T.; Sonoyama, N.; Yamada, A.; Kondo, S.; Nagao, M.; Kanno, R. *J. Power Sources* **2009**, *194*, 1085−1088.
(43) Ito, S.; Fujiki, S.; Yamada, T.; Aihara, Y.; Park, Y.; Kim, T. Y.; Baek, S.-W.; Lee, J.-M.; Doo, S.; Machida, N. *J. Power Sources* **2014**, *248*, 943−950.
(44) Seol, J.-H.; Won, J.-H.; Yoon, K.-S.; Hong, Y. T.; Lee, S.-Y. *Solid State Ionics* **2011**, *190*, 30−37.
(45) Every, H. A.; Janssen, G. J. M.; Sitters, E. F.; Mendes, E.; Picken, S. J. *J. Power Sources* **2006**, *162*, 380−387.
(46) Mercier, R.; Malugani, J.-P.; Fahys, B.; Robert, G.; Douglade, J. *Acta Crystallogr.* **1982**, *B38*, 1887−1890.
(47) Kuhn, A.; Koehler, J.; Lotsch, B. V. *Phys. Chem. Chem. Phys.* **2013**, *15*, 11620−11622.
(48) Lee, S.-Y.; Choi, K.-H.; Choi, W.-S.; Kwon, Y. H.; Jung, H.-R.; Shin, H.-C.; Kim, J. Y. *Energy Environ. Sci.* **2013**, *6*, 2414−2423.
(49) Koo, M.; Park, K.-I.; Lee, S. H.; Suh, M.; Jeon, D. Y.; Choi, J. W.; Kang, K.; Lee, K. J. *Nano Lett.* **2012**, *12*, 4810−4816.
(50) Jung, Y. S.; Cavanagh, A. S.; Gedvilas, L.; Widjonarko, N. E.; Scott, I. D.; Lee, S. H.; Kim, G. H.; George, S. M.; Dillon, A. C. *Adv. Energy Mater.* **2012**, *2*, 1022−1027.
(51) Zaban, A.; Zinigrad, E.; Aurbach, D. *J. Phys. Chem.* **1996**, *100*, 3089−3101.
(52) Girishkumar, G.; McCloskey, B.; Luntz, A. C.; Swanson, S.; Wilcke, W. *J. Phys. Chem. Lett.* **2010**, *1*, 2193−2203.

DOI: 10.1021/acs.nanolett.5b00538
Nano Lett. 2015, 15, 3317−3323